PAUDLER, W. W., ZEILER, A. G. & GAPSKI, G. R. (1969). *J. Org. Chem.* **34**, 1001–1004.

ROYER, D. J., SCHIEVELBEIN, V. H., KALYANARAMAN, A. R. & BERTRAND, J. A. (1972). *Inorg. Chim. Acta*, **6**, 307–313.

SAYRE, D. (1952). *Acta Cryst.* **5**, 60–65.

SCHENK, H. (1971). *Acta Cryst.* **B27**, 185–188.

SMITH, G. D. (1968). Cell Dimensions Least-Squares Program, Ohio Univ. Crystallography Laboratory, Athens, Ohio.

SMITH, G. D., FITZGERALD, A., CAUGHLAN, C. N., KERR, K. A. & ASHMORE, J. P. (1974). *Acta Cryst.* **B30**, 1760–1766.

STANISLOWSKI, A. & FRENZ, B. (1973). Program *HYDROGEN*, Texas A. & M. Univ. Crystallographic Computing Library, College Station, Texas.

STOUT, G. H. & JENSEN, L. H. (1968). *X-ray Structure Determination*, pp. 420–421. New York: Macmillan.

WIBERG, K. B. (1965). *J. Amer. Chem. Soc.* **87**, 1070–1078.

Rotation Function Studies of Southern Bean Mosaic Virus at 22 Å Resolution

BY JOHN E. JOHNSON, PATRICK ARGOS* AND MICHAEL G. ROSSMANN

Department of Biological Sciences, Purdue University, West Lafayette, Indiana 47907, U.S.A.

Approximately 60% of the data to a resolution of 22 Å has been collected for an $R32$ form of southern bean mosaic virus. The data were used to compute the rotation function for fivefold, fourfold, threefold, and twofold symmetry axes. An orientation of the icosahedral virus was determined consistent with the observed function. This differed from an earlier prediction based on apparent spikes of an $hk0$ photograph.

Introduction

Southern bean mosaic virus (SBMV) is a small spherical plant virus of molecular weight $6\cdot6 \times 10^6$ daltons (Miller & Price, 1946) containing 21% RNA by mass (Ghabrial, Shepherd & Grogan, 1967). The single protein component in the coat (Hill & Shepherd, 1971) has a molecular weight of 29000 daltons consistent with the presence of 180 protein subunits in the virus and $T=3$ icosahedral symmetry (Caspar & Klug, 1962). A number of crystalline forms of SBMV have been obtained. Magdoff (1960) reported an orthorhombic form of space group $C222_1$ with $a=295$, $b=508$, $c=474$ Å. In this laboratory three different crystalline forms have been obtained: type I in space group $R32$ with $a=542$ Å, $\alpha=116°42'$ (Johnson, Rossmann, Smiley & Wagner, 1974); type II in space group $R32$ with $a=317$ Å, $\alpha=62°30'$; and type III in space group $C222_1$ with $a=335$, $b=530$, $c=530$ Å (Akimoto, Wagner, Johnson & Rossmann, 1975). In the type I crystal form there are three virus particles in the rhombohedral cell and each particle must therefore have one of its twofold axes directed along a crystallographic a axis of the hexagonal unit cell (Fig. 1). An orientation of the particle about the crystallographic twofold axis was previously suggested on the basis of apparent spikes observed on an $hk0$ precession photograph (Johnson *et al.*, 1974). These conclusions were, however, based on inadequate experimental data.

---

* Present address: Department of Physics, Southern Illinois University, Edwardsville, Illinois 62025, U.S.A.

Subsequently a data set consisting of approximately 60% of the 22 Å data was collected and used to calculate the rotation function (Rossmann & Blow, 1962).

Reported here are the details of the data collection and a revised particle orientation which was obtained by computing a rotation function with these three-dimensional data.

Experimental

Rhombohedral type I crystals were obtained with techniques previously described (Johnson *et al.*, 1974). The crystal morphology necessitated the placement of the $[hh0]$ axis along the camera spindle axis. (Reference to this crystal lattice will be in terms of the hexagonal unit cell with $a=923$, $c=302$ Å.) Data were collected with standard precession techniques and a crystal-to-film distance of 100 mm. However, a layer-line screen with a 3 mm radius hole, rather than an annulus, was used to block upper-layer reciprocal-lattice reflections. The negative reciprocal-lattice levels did not intersect the sphere of reflection at the small precession angles for the chosen zones.

A total of 18 zero level $\mu=2°0'$ precession photographs (Fig. 2) were taken with Ni filtered Cu $K\alpha$ radiation using a $0\cdot2$ mm collimator. Intensity measurements were made with an Optronics photoscan film scanner. The film scanner procedure (Ford, 1974) calculated the intensity of a reflection by a profile-fitting method. Different films within one film pack, symmetry-related reflections within one plane and different film planes were successively scaled together by the method of Hamilton, Rollett & Sparks (1965).

Results of scaling 16 of the 18 film packs together gave a residual of $r = 17\%$ where

$$r = \sum_{h} \left\{ \frac{\sum_{i=1}^{n} |(I_{hi} - I_h)|}{n} \right\} / \sum I_n$$

and I_h is the mean of the n reflections I_{hi} on film $i = 1, 2, \ldots, n$. (Two of the films contained no significant data.) 376 independent reflections (60% of all such reflections) were found to be greater than two standard deviations above background.

The three basic variables in the computation of the rotation function (Rossmann & Blow, 1962) are the cut-off limits for the resolution of the data, the radius of integration with its associated problem of series termination, and the number of terms to be used in the representation of the rotated Patterson synthesis. These parameters were determined experimentally to obtain reasonable peak-to-background ratios in the observed function. They were checked with data from model structures by calculating corresponding rotation functions. The radius of integration was then chosen to be 100 Å, rather less than the particle diameter of 280 Å. The resolution limits were set between 40 and 22 Å, corresponding to the experiences of Lentz & Strandberg (1974) with a rotation function for satellite tobacco necrosis virus (STNV). The rotated Patterson synthesis was represented by the 46 largest terms of the observed 376 coefficients.

The spherical polar coordinate system used for computation of the rotation function is that defined by Rossmann & Blow (1962). Another variable, θ, was used in defining the orientation of each icosahedron about its crystallographic twofold axis (Fig. 3). Rotation function sections were initially computed for $\kappa = 180°$, 144°, 120° and 72° in a search for non-crystallographic icosahedral rotations of $\frac{1}{2}$, $\frac{2}{5}$, $\frac{1}{3}$ and $\frac{1}{5}$ of (2π). A particularly dominant set of peaks was observed to correspond to two sets of octahedra related by a rotation of 60° about the crystallographic c axis. This was then found to be consistent with a subsequent computation of the $\kappa = 90°$ section.
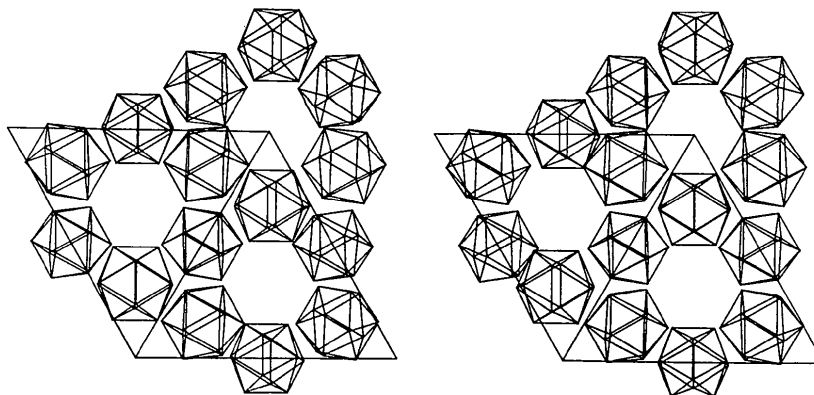
Interpretation of the observed rotation function

Peaks can arise in the rotation function from three sources (Lentz & Strandberg, 1974): (1) symmetry elements within the virus particle, to be termed here 'particle peaks'; (2) pseudo-symmetry elements relating one particle to another in the real crystal lattice when the particles are considered to be spherically averaged, to be termed here 'packing peaks'; (3) symmetry elements that are generated by superimposing the self-Pattersons of crystallographically related particles at a common origin. The latter have been termed 'packing peaks' (Klug, 1971) but will be referred to here as 'Klug peaks'. Klug peaks are absent if there is only one orientation of the particle in the unit cell as in tomato bushy stunt virus (Harrison, 1971). The analysis of the rotation function in terms of these three types of peaks will now be considered.

(1) Particle peaks

Owing to the crystallographic symmetry, the SBMV particles are found in three orientations. There is, however, only one degree of rotational freedom, that
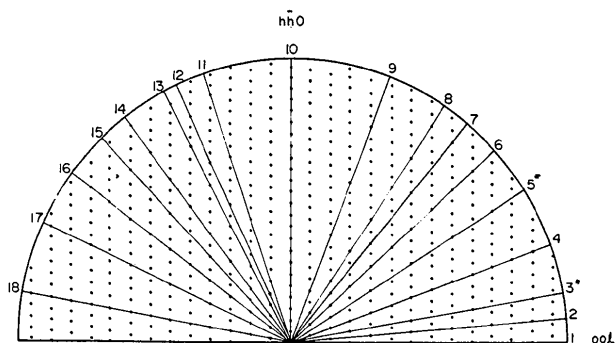

Fig. 2. Scheme for collecting 22 Å data for type I SBMV crystals consisting of 18 zero-level zones. The diagram is shown projected along the [hh0] axis which was placed along the camera spindle. The zones marked with an asterisk did not contain a significant number of observed reflections. The threefold axis along [00l] allows 60% of the data to be observed.

Fig. 1. Stereo view of packing of icosahedra within the hexagonal unit cell.

being about any of the crystallographic twofold axes. Fig. 4 is a stereogram of the symmetry elements for an icosahedron in a single orientation. Fig. 5 depicts the threefold superposition of symmetry elements generated from an icosahedron oriented as in Fig. 4. The chosen icosahedral orientation was that which best satisfied the observed rotation function (Figs. 6, 7, 8 and 10). This orientation differs from that previously reported (Johnson *et al.*, 1974) by a rotation of roughly 90° in θ.

To check systematically all possibilities, each orientation was tested by sampling the rotation function at
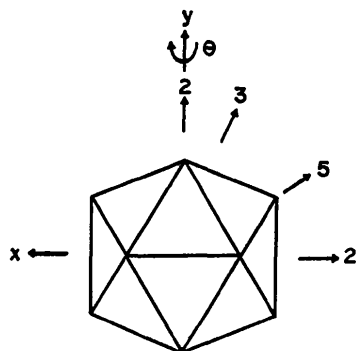

Fig. 3. Definition of angle θ which gives the orientation of an icosahedron about the crystallographic twofold axis. Diagram shows view of particle in relation to the set of right-handed Cartesian coordinates defined with respect to the crystal axis as by Rossmann & Blow (1962). Positive θ corresponds to a clockwise rotation about y while looking into the y axis. The particle in the diagram is positioned at $\theta = 0°$, corresponding to the particle twofold axis parallel to the crystallographic threefold axis.
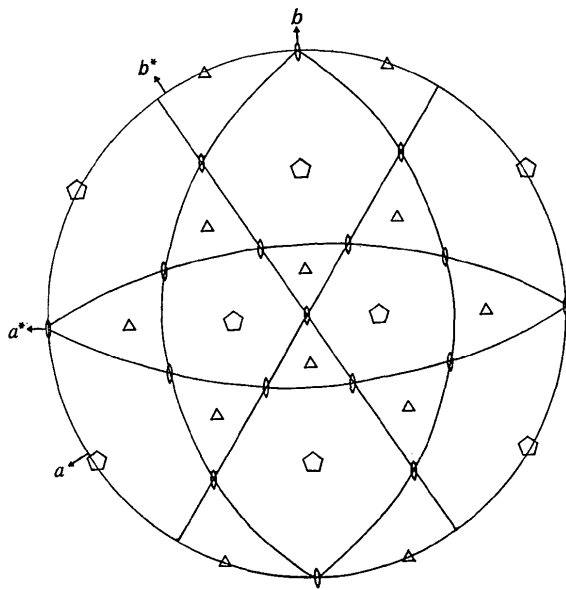

Fig. 4. Stereographic projection of the symmetry elements of an icosahedron at $(0, \frac{1}{2}, 0)$ in the orientation consistent with the rotation function.
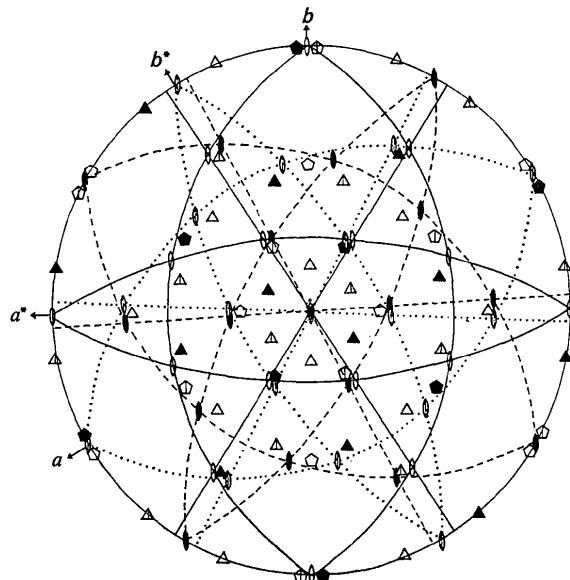

Fig. 5. Stereographic projection of the symmetry elements for three icosahedra in an orientation consistent with the rotation function results. The solid great circles pass through the twofold axes of the icosahedron oriented as in Fig. 4, while the dashed and dotted great circles pass through twofold axes of icosahedra related to that in Fig. 4 by a threefold rotation about the c axis directed into the page.
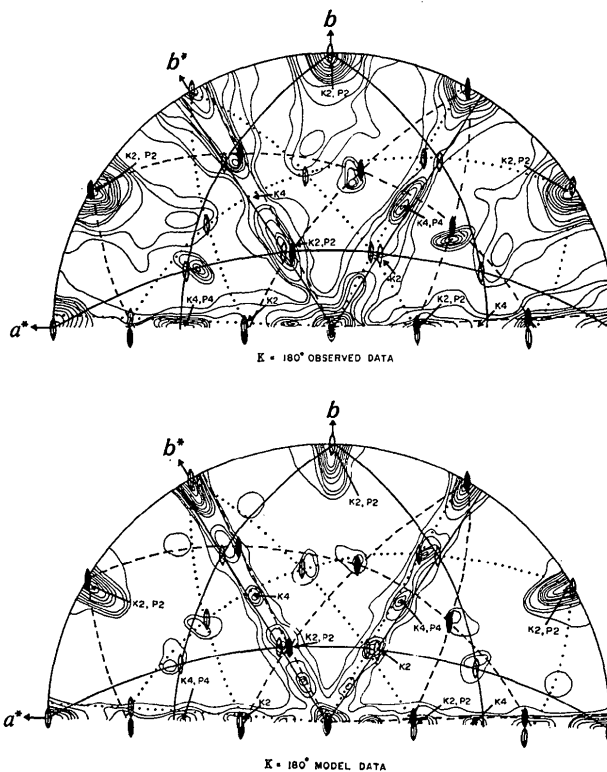

Fig. 6. Stereographic projection of the rotation functions computed with observed (above) and model data (below) for $\kappa = 180°$. Contours are at arbitrary equal intervals. K2 and K4 are Klug twofold and fourfold peaks while P2 and P4 are packing twofold and fourfold peaks, respectively.

the position of every noncrystallographic symmetry element generated by the three related icosahedra. The plot of this 'locked rotation function' (Rossmann, 1972a) is shown in Fig. 11. Since the sampling of each section alone gave very similar results, Fig. 11 shows only the composite result for all values of θ. The maximum was found to be at $\theta = -3\cdot5 \pm 2°$.

Although the locked rotation function determined a unique orientation of the icosahedra, the octahedral peaks in the original rotation function were without satisfactory interpretation. It was therefore necessary to show that their size and position were consistent with either 'packing' or 'Klug' peaks.

(2) Packing peaks

If four particles per cell were present in the SBMV rhombohedral crystals (Johnson et al., 1974), rather than the three found, a pseudo body-centered cubic packing would result. Such a cubic arrangement of spheres (even in the absence of some of the particles as in the present case) would be consistent with one of the two sets of octahedrally distributed peaks in the rotation function. These have been marked P2, P3 and P4 on Figs. 6, 8 and 9 corresponding to twofold, threefold and fourfold packing peaks. Nevertheless, the height of these peaks is greater than might be expected for particles of diameter 280 Å examined with 22 Å resolution data (see below).

(3) Klug peaks

Inspection of Fig. 12 shows a distribution of pseudo-symmetry elements corresponding to two sets of octahedra (one of these is coincident with the octahedral distribution of packing peaks) consistent with those found in the rotation function (Figs. 6, 8 and 9). Unlike the similar case encountered in the study of STNV (Åkervall et al., 1971), these noncrystallographic symmetry elements relate only parts of the different self-Pattersons to each other.

Thus it can be concluded that the large octahedrally distributed peaks in the rotation function are partially due to packing peaks and (more important) due to Klug peaks. Many of these peaks are also coincident with particle peaks.

Comparison with model structures

In order to compare systematically the heights of the different types of peaks, the rotation functions for three different model structures were computed. These corresponded to (a) the orientation that was previously suggested by Johnson et al. (1974) corresponding to $\theta = 90°$; (b) an orientation close to that found here, with $\theta = 0°$; and (c) the particle icosahedral threefold axis parallel to (but not coincident with) the crystallographic threefold axis, with $\theta = -69°$. The model (c) was suggested on the basis of visual inspection of the rotation function and spikes in the diffraction pattern.
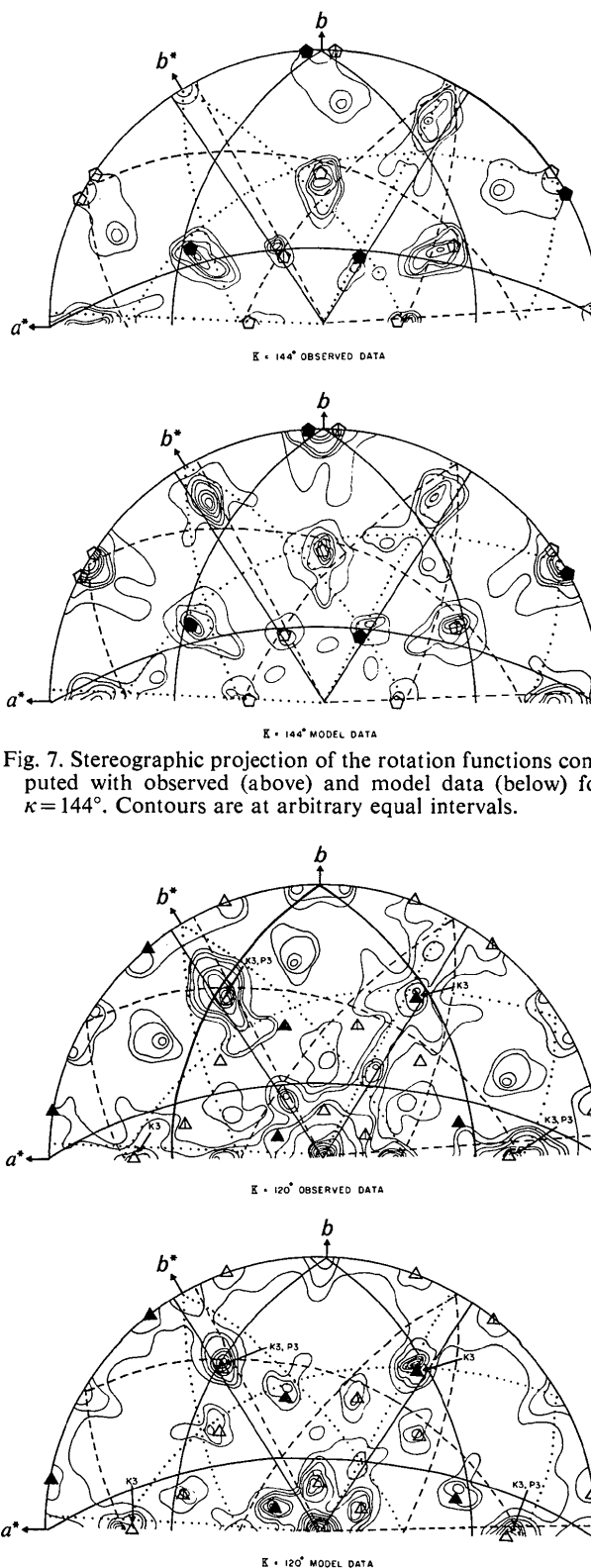

Fig. 7. Stereographic projection of the rotation functions computed with observed (above) and model data (below) for $\kappa = 144°$. Contours are at arbitrary equal intervals.

Fig. 8. Stereographic projection of the rotation functions computed with observed (above) and model data (below) for $\kappa = 120°$. Contours are at arbitrary equal intervals. K3 and P3 are Klug and packing threefold peaks, respectively.
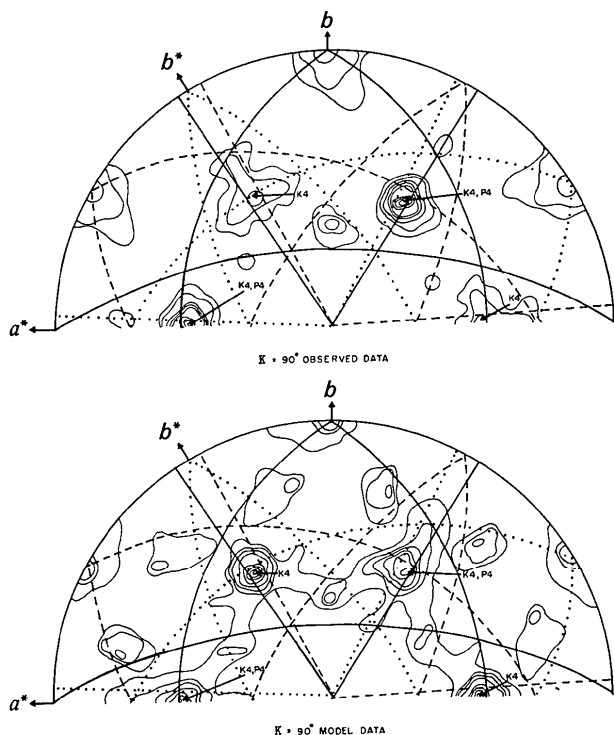
The octahedral peaks were compared with single noncrystallographic particle symmetry peaks. Particular attention was paid to the fourfold peak at $\kappa = 90°$, $\psi = 45°$, $\varphi = 55°$ as it cannot be coincident with any icosahedral particle peaks. The model structures permitted the uncoupling of the contributions of 'Klug' and 'packing' peaks, since only in model (b) is the set of 'packing' peaks coincident with a set of 'Klug' peaks.

Fig. 9. Stereographic projection of the rotation functions computed with observed (above) and model data (below) for $\kappa = 90°$. Contours are at arbitrary equal intervals. K4 and P4 are Klug and packing fourfold peaks, respectively.
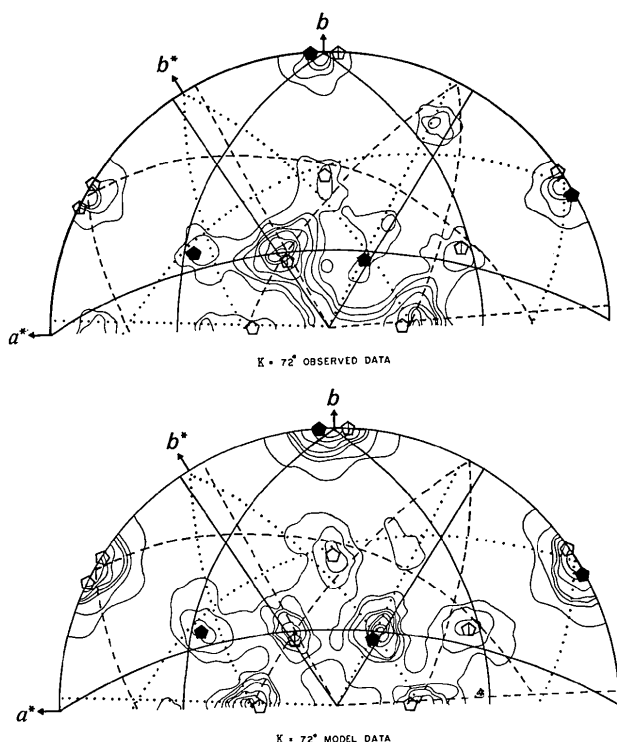

Fig. 10. Stereographic projection of the rotation functions computed with observed (above) and model data (below) for $\kappa = 72°$. Contours are at arbitrary equal intervals.

Table 1. *Peak heights in rotation functions for three different models compared with those in the observed function*

Type of peak	Mean height	Number of independent observations
Model (a), $\theta = 90°$		
Origin	100	1
Particle peaks		
$\kappa = 180°$, single peak	29	2
$\kappa = 180°$, double peak	46	2
$\kappa = 120°$	28	3
$\kappa = 72°, 144°$	not computed	
Klug peaks		
$\kappa = 180°$ }	{ identical with	
$\kappa = 120°$ }	{ particle peaks	
$\kappa = 90°$	54·3	1
Packing peaks		
$\kappa = 180°$	15	1
$\kappa = 120°$	13	1
$\kappa = 90°$	13	1
Model (b), $\theta = 0°$		
Origin	100	1
Particle peaks		
$\kappa = 180°$, single peak	21	2
$\kappa = 180°$, double peak	42	2
$\kappa = 120°$	23	3
$\kappa = 72°, 144°$	39	4
Klug peaks		
$\kappa = 180°$ }	{ identical with	
$\kappa = 120°$ }	{ particle peaks	
$\kappa = 90°$	48	1
Packing peaks	{ coincident with Klug peaks	
Model (c), $\theta = -69°$		
Origin	100	1
Particle peaks		
$\kappa = 180°$, triple peak	71	3
$\kappa = 120°$, triple peak	68	2
$\kappa = 72°, 144°$, triple peak	69	2
Klug peaks	do not exist	
Packing peaks		
$\kappa = 180°$	21	1
$\kappa = 120°$	13	1
$\kappa = 90°$	22	1
Observed function		
Origin	100	1
Particle peaks		
$\kappa = 180°$, single peak	15	2
$\kappa = 180°$, double peak	26	2
$\kappa = 120°$	9	3
$\kappa = 72°, 144°$	17	4
Klug peaks		
$\kappa = 180°$ }	{ coincident with	
$\kappa = 120°$ }	{ particle peaks	
$\kappa = 90°$	36	1
Packing peaks	{ coincident with Klug peaks	

A model virus particle was designed to exhibit only the $T=3$ icosahedral symmetry of the protein coat. The protein subunits consisted of spheres 20 Å in diameter of uniform density. A total of 180 such symmetrically arranged spheres were in contact when the distance from the center of the virus to the center of the coat protein subunit was 124 Å. The model virus was rotated to the desired orientation, placed in the $R32$ unit cell and a 30 Å data set generated. The rotation function was then computed using data from 50 to 30 Å resolution and a radius of integration of 100 Å.

Table 1 gives an analysis of the heights for various types of peaks, related to the model structures (a), (b), and (c). It also shows a similar analysis for the observed rotation function. In models (a) and (c), the Klug, packing and noncrystallographic particle peaks are generally separated from one another, although double and triple noncrystallographic particle peaks are encountered. In model (b), corresponding to the interpretation of the observed function, packing peaks are always in coincidence with Klug peaks and sometimes also superimposed on a noncrystallographic particle peak.

Inspection of Table 1 shows that for any one model single and double particle peaks are roughly in the ratio of $1:2$. In model (a), where the Klug and packing peaks are separated, the Klug peaks are about double a single particle peak and the packing peaks are about one-half of a single particle peak. In model (c) where there are no Klug peaks, the packing peaks are slightly less than the value expected for a single particle peak. However, the size of packing peaks is strongly dependent upon the distribution of large terms selected for the rotation function. Thus with fewer terms, the tendency is to emphasize the larger lower-order reflections which will enhance the packing effect. In model (b), where packing peaks are coincident with Klug peaks, these combined peaks are roughly double single particle peaks, showing again the dominant Klug effect as opposed to the packing effect. The observed results given in Table 1 are similar to those for model (b) but quite unlike those for model (c). Although the size of the Klug peaks are similar for models (a) and (b) they are in completely different positions on the rotation function. Thus these three models are clearly distinguishable.

Distribution of strong intensity spikes in reciprocal space

Since the orientation originally predicted for SBMV was based upon spikes observed on the $hk0$ photograph, it is necessary to explain how these led to a wrong interpretation and to correlate spikes observed on various other photographs with symmetry elements consistent with the rotation function results.

The $hk0$ photograph initially analyzed (Johnson et al., 1974) for spikes was taken on a standard fine-focus X-ray tube with a 400 μm target width. When

this same zone was re-photographed with the more intense X-ray source provided by a rotating anode tube with a 200 μm focal spot, the spikes were no longer obvious. Spikes on other zones were, however, sharper and far more intense. The orientations of all these spikes were plotted on a stereogram. The spindle angle for the photograph determines the great circle upon which the spike must lie, while the angle from the
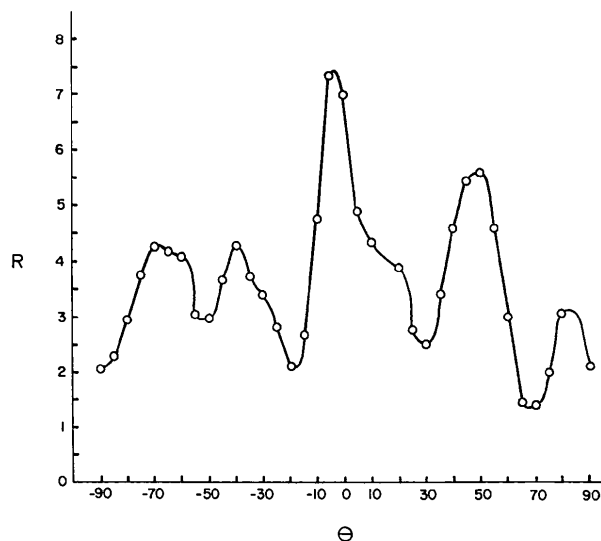

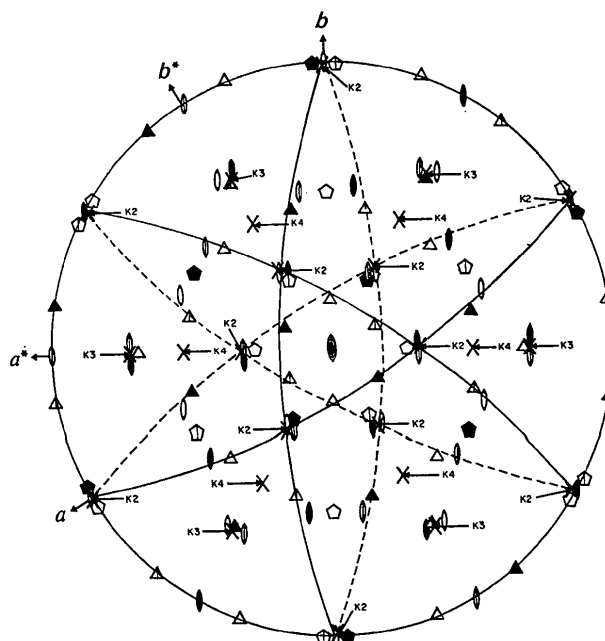Fig. 11. Plot of the locked rotation function against the rotation angle θ as defined in Fig. 3.

Fig. 12. Distribution of icosahedral symmetry elements showing their octahedral relationship. The resultant octahedral Klug symmetry positions are marked K2, K3 and K4 for two-, three- and fourfold axes. The great circles pass through the twofold octahedral positions.
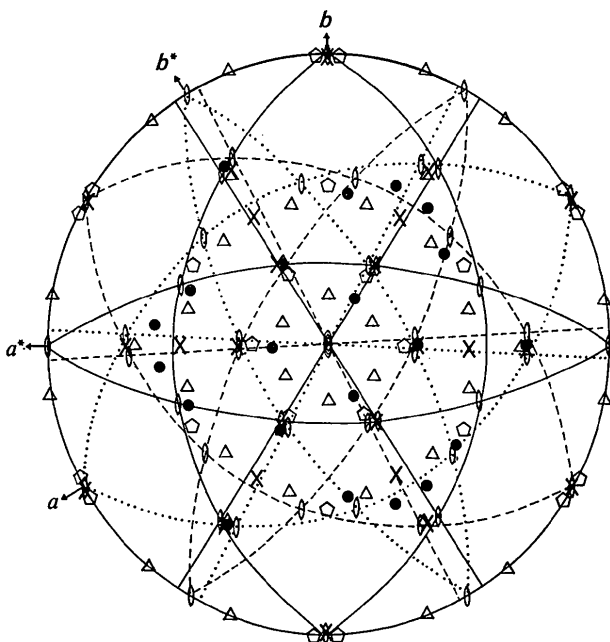
Fig. 13. Stereographic plot of position of high intensity spikes (black dots) observed on diffraction photographs. Predicted particle and Klug symmetry elements are shown for comparison.
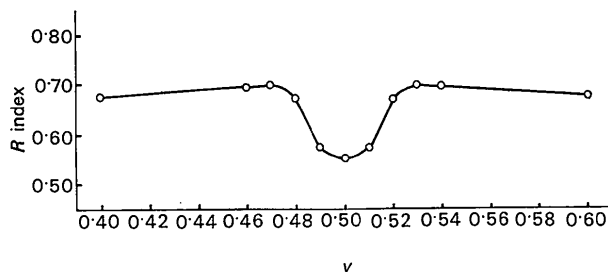

Fig. 14. Plot of the conventional crystallographic R index as a function of the fractional y coordinate in the vicinity of $y=\frac{1}{2}$. A uniform density sphere of diameter 280 Å was used for a model. Data to a resolution of 40 Å were employed. The agreement index at the other sterically reasonable virus position, $y=0\cdot17$, was $0\cdot76$.

spindle axis to the spike on the photograph determines the small circle. The coincidence of spikes with positions of multiple symmetry elements is quite clear (Fig. 13), although spikes associated with single symmetry elements are not very intense.

The orientation of the particle corresponding to model (c) also fits the spike distribution quite well. The peak heights observed on the rotation function, however, clearly differentiate this model from the correct solution (see above).

The position of the particle within the crystal

It has already been reported (Johnson *et al.*, 1974) that a particle must sit on the *b* axis close to $y=\frac{1}{2}$, and related space-group equivalent positions. To deter-

mine the exact position of the particle an R-index search was made employing 40 Å data and a model uniformly dense sphere of diameter 280 Å. Fig. 14 shows the exploration of the translation parameter as a function of the residual. The results clearly show that $y=0\cdot50\pm0\cdot01$.

Conclusion

The orientation and position of the virus particle in the crystal unit cell has now been established to within the limits of error provided by the 22 Å resolution data (Fig. 1). With these parameters it is possible to apply the methods of molecular replacement (Rossmann, 1972b; Bricogne, 1974) in determining phases for the 22 Å data set. This structure can then serve as a phasing model to the recently produced SBMV type II crystals (Akimoto *et al.*, 1975) for which the diffraction pattern extends to high resolution.

References

AKIMOTO, T., WAGNER, M. A., JOHNSON, J. E. & ROSSMANN, M. G. (1975). *J. Ultrastruct. Res.* In the press.
BRICOGNE, G. (1974). *Acta Cryst.* A**30**, 395–405.
CASPAR, D. L. D. & KLUG, A. (1962). *Cold Spring Harbor Symp. Quant. Biol.* **27**, 1–24.
FORD, G. C. (1974). *J. Appl. Cryst.* **7**, 555–564.
GHABRIAL, S. A., SHEPHERD, R. J. & GROGAN, R. G. (1967). *Virology*, **33**, 17–25.
HAMILTON, W. C., ROLLETT, J. S. & SPARKS, R. A. (1965). *Acta Cryst.* **18**, 129–130.
HARRISON, S. C. (1971). *Cold Spring Harbor Symp. Quant. Biol.* **36**, 495–501.
HILL, J. H. & SHEPHERD, R. J. (1971). *Phytopathology*, **61**, 1408–1409.
JOHNSON, J. E., ROSSMANN, M. G., SMILEY, I. E. & WAGNER, M. A. (1974). *J. Ultrastruct. Res.* **46**, 441–451.
KLUG, A. (1971). *Cold Spring Harbor Symp. Quant. Biol.* **36**, 483–487.
LENTZ, P. J. JR & STRANDBERG, B. (1974). *Acta Cryst.* A**30**, 552–559.
MAGDOFF, B. S. (1960). *Nature, Lond.* **185**, 673–674.
MILLER, G. L. & PRICE, W. C. (1946). *Arch. Biochem.* **10**, 467–477.
ROSSMANN, M. G. (1972a). *J. Mol. Biol.* **64**, 246–247.
ROSSMANN, M. G. (1972b). *The Molecular Replacement Method*. New York: Gordon and Breach.
ROSSMANN, M. G. & BLOW, D. M. (1962). *Acta Cryst.* **15**, 24–31.
ÅKERVALL, K., STRANDBERG, B., ROSSMANN, M. G., BENGTSSON, U., FRIDBORG, K., JOHANNISEN, H., KANNAN, K. K., LÖVGREN, S., PETEF, G., ÖBERG, B., EAKER, D., HJERTÉN, S., RYDÉN, L. & MORING, I. (1971). *Cold Spring Harbor Symp. Quant. Biol.* **36**, 469–483.